Inhibition of Micro-pitting by Tribofilm-forming ZrO2 Nanocrystal Lubricant Additives: A Micro-pitting Rig and Transmission Electron Microscope Study

Imène Lahouij (imene.lahouij@mines-paristech.fr)
MINES ParisTech - Sophia Antipolis
Benjamin Gould
Argonne National Laboratory
Nicholaos G Demas
Argonne National Laboratory
Aaron C Greco
Argonne National Laboratory
Zhiyun Chen
Pixelligent Technologies LLC
Gregory D Cooper
Pixelligent Technologies LLC
Andrew Jackson
University of Pennsylvania School of Engineering and Applied Science
Robert W Carpick
University of Pennsylvania School of Engineering and Applied Science

Research Article

Keywords: ZrO2 Nanocrystal, Lubricant, Anti-Wear, Micro-pitting, Transmission Electron Microscopy (TEM)

Posted Date: October 19th, 2021

DOI: https://doi.org/10.21203/rs.3.rs-976353/v1

Version of Record: A version of this preprint was published at Tribology Letters on January 6th, 2022. See the published version at https://doi.org/10.1007/s11249-021-01555-2.

Abstract

The drive to reduce fuel consumption in transportation has encouraged the emergence of low viscosity lubricants to reduce viscous losses in the engine, drivetrain, and other components. However, viscosity reduction increases the risk of surface damage, thus motivating the development of new anti-wear (AW) additives. Capped ZrO2 nanocrystals (NCs) in base oils have been shown to form AW tribofilms within microscale sliding contacts. However, the potential of ZrO2 NCs to protect surfaces subjected to rolling-sliding contact from macroscale damage, such as micro-pitting, remains unexplored. Here, we explore the ability of ZrO_2 NCs to form protective tribofilms under harsh conditions using a micro-pitting rig (MPR), consisting of a three ring-on-roller configuration. The experiments were conducted in polyalphaolephin (PAO) base oil, with and without 5 nm diameter ZrO2 NCs, at two levels of slide-to-roll ratio (SRR) (30% and 0%) and at variable test durations up to long durations (119 hours). MPR results showed the use of ZrO_2 NCs gives rise to the formation of a tribofilm covering the roller surfaces and decreases the initiation and propagation of micro-pits compared to tests in pure PAO base stock. Transmission electron microscopy (TEM) performed on focused ion beam (FIB) milled cross-sectional samples of the roller surfaces revealed the growth of dense and 50- 100 nm thick ZrO_2-based tribofilms independent of (SRR), indicating the potential for robust micro-pitting fatigue protection. Nevertheless, small cracks localized within the near surface region of the roller tested at the most severe conditions (30% SRR and 119 hours) were observed. The initiation of these cracks was directly related to the presence of manganese sulphide (MnS) inclusions in the steel, revealed using TEM combined with energy dispersive spectroscopy (EDS). The results highlight the benefits of the protective tribofilms formed by ZrO_2 NCs and suggest approaches for further optimizing their use.

Introduction

Growing concerns about climate change and environmental impact have encouraged researchers to improve energy efficiency in every technological field. In the automotive industry, the push to increase energy efficiency includes advancing the use of low viscosity (LV) lubricants, which reduce viscous drag of mechanical components in contact with one and other. Recent studies, from bench tests to full vehicle tests, have concluded that lower viscosity lubricants in engines, drivetrains, and other components can lead to significant reductions in CO_2 emissions [1]. However, as lubricant viscosity decreases, so does the thickness of the hydrodynamic film generated by the lubricant, thereby leading to more mixed and boundary contact, and thus an increase in various forms of surface damage.

Surface initiated damage modes, such as micro-pitting and surface initiated macro-pitting can be driven by stress fluctuations due to asperity interactions in rolling-sliding contacts. Cyclic loading results in fatigue damage accumulation in the near-surface region, giving rise to the initiation of surface or near-surface fatigue cracks. These cracks then propagate under stress from the surface into the material at a shallow angle until rupture occurs, resulting in pits typically tens of μm deep [2–3]. Micro-pitting is a common failure mode in numerous tribological components including but not limited to gears, rolling

bearings, and the surfaces of cams and tappets. Multiple factors influence the surface contact fatigue phenomena involved including specific film thickness [4–5], contact pressure [6], slide-to-roll ratio [7–8], surface roughness [9–10], surface defects and inclusions [11–12–13], and lubricants including both base oil and additives [14–15–16]. The specific film thickness λ, defined as the lubricant film thickness over the surface root mean squared (RMS) roughness, is considered as the controlling parameter for surface fatigue processes [17]. The use of LV oils implies a decrease of the specific film thickness, resulting in an increase of direct asperity contact along with high stress concentrations, which raise the risk of surface fatigue. Therefore, the role of additives becomes crucial in regard of surface damage.

Anti-wear (AW) and extreme pressure (EP) additives, typically incorporated in engine and drivetrain lubricants, are of additional importance for LV lubricants so as to mitigate the damage caused by the increased degree of operation under boundary lubrication conditions. These additives extend the wear-limited service life of mechanical components. However, the effect that these additives have on the initiation and propagation of surface cracks is not completely understood. Several studies have shown improvements in the rolling contact fatigue behavior when AW and EP additives are used [18–19–20–21]. Evans et al. [22–23] showed that the addition of S- and P-containing additives to mineral oil inhibited the formation of cracks in the near surface of roller bearing cones through the formation of an AW surface layer rich in Fe, P, S, and O. In addition, transmission electron microscopy (TEM) imaging revealed a sharp interface between the AW surface layer and the underlying steel, suggesting the removal of the initial surface asperities which resulted in a smoother contact and a decrease in stress concentrations. It was also documented that the elements in the AW layer did not diffuse into the near surface region of the steel, or attack grain boundaries. The exact AW surface-layer formation mechanism from S- and P-containing additives in gear oils was not established. However, similarities between the AW layer and ZDDP film deposition schematic models [24–25] were discussed. On the other hand, a number of studies have shown a detrimental effect of S- and P-containing AW and EP additives on pitting life, which is linked to their chemical reactivity that leads them to attack the metal surface, promoting crack initiation by the creation of corrosion pits [26–27–28–29]. It was demonstrated that the effect of additives on the fatigue life depends on their concentrations in oil and on their chemical reactivity [16–30–31].

Ueda et al. [32] recently investigated the effect of ZDDP concentration on micro-pitting and surface fatigue. A correlation between AW tribofilm growth rate and micro-pitting was observed. It was postulated that the formation of a thick AW tribofilm early in the test served to prevent adequate running-in of the sliding components. This subsequently led to higher asperity stresses, resulting in an increase in micro-pitting. The establishment of this correlation is of significant interest in the design of efficient oil formulations by controlling both wear and micro-pitting damage, since some degree of run-in before a protective tribofilm forms may be desirable.

The potential of nanoparticles as an eco-friendly alternative to S- and P-containing additives to enhance friction behavior and wear resistance has been widely studied for a range of lubricants [33–34–35–36]. However, the effects of NPs on the rolling contact fatigue life are not well known. Rico et al. [37] have shown that the addition of polytetrafluoroethylene (PTFE) nanoparticles in both mineral and synthetic

base stocks, at concentrations lower than 3%, increased the fatigue life of steel. The authors measured the contact angle between the counterparts and found that it decreased in the presence of PTFE. This led them to conclude that these nanoparticles improve adsorption phenomena, and possibly increasing the oiliness of the lubricant. They also claimed that mechanical interposition of PTFE particles between the surfaces could protect them from fatigue. However, no surface analyses were performed to observe the presence of cracks at the contact. Aldana et al. [38] have shown that WS_2 NPs when added to base oil increase the life span of gear drives. Energy dispersive spectroscopy (EDS) analyses in a TEM revealed the presence of a tungsten- and sulfur-containing tribofilm on the surface of the gear tooth as well as all along the wall of the cracks. These observations suggest that nanoparticles are able to ingress into surface cracks, and may have a sealing effect, reducing the propagation of cracks and preventing the mechanical part from early failure. Furthermore, a synergistic ability to mitigate cracking damage was documented between WS_2 NPs and the fully formulated additive package used in testing. More recently, the micro-pitting and wear performance of CuO NPs and WC NPs in base oil containing oleic acid surfactant were investigated using a micro-pitting test rig (MPR) [39]. It was found that both NPs exhibited increased micro-pitting life compared to the base stock, although nanofluid containing WC NPs showed significantly improved performance in reducing micro-pitting, wear, and the traction coefficient. Based on scanning electron microscopy (SEM) analysis of the surface rollers, it was proposed that WC NPs form a protective tribofilm, while CuO NPs filled the surface cracks to some extent, which delayed the propagation of micro-pitting after certain number of cycles. However, further analyses of contact surfaces in depth are required to confirm the mechanisms by which these NPs operate to inhibit the propagation of cracks and pits.

Therefore, nanoparticle additives have shown promise to increase fatigue life of rolling-sliding contacts which motivates further investigations in this direction. We have previously shown the potential of ligand-capped 5 nm-diameter ZrO_2 nanocrystals (NCs; referred to as such as they are single crystal) to form robust AW tribofilm across a broad range of conditions in both base oils [40–41–42] and alongside co-additives [43]. The film formation is attributed to tribosintering, whereby the capping ligands are removed when the NCs are entrained into the contact, and the bare NC's bond to the steel surface and to each other, forming a solid film. Using an *in situ* AFM tribometer method supplemented with TEM characterization, it was found that growth of a dense, solid, nanocrystalline, surface-bound ZrO_2 tribofilm occurs across temperatures from −25 to 100°C at pure sliding contact conditions. The surface roughness drives tribofilm nucleation whereas contact stress favorites the tribofilm growth rate [41]. Furthermore, the addition of ZrO_2 in a fully formulated 75W-80 gear oil was found to reduce underlying surface wear across a range of slide-to-roll ratios, including rolling conditions (0% SRR) [43]. More recently, a ball-on-disc tribometer was used to investigate the formation rate of tribofilms formed by ZrO_2 dispersed in PAO4 at SRR 50% and over a range of applied loads in the boundary lubrication regime [44]. A linear correlation was found between the tribofilm growth rate and the applied normal load supporting the hypothesis of a tribosintering process of ZrO_2 tribofilms.

In this work, we evaluate the performance of the capped ZrO_2 NCs under severe rolling-sliding contact conditions. Using a micro-pitting rig (MPR) tribometer, a low viscosity base oil (PAO4) is tested with and without ZrO_2 NCs, each at two SRR levels. In-depth cross-section analyses combining focused ion beam (FIB) with analytical TEM techniques are used to investigate the ability of ZrO_2 NCs to prevent surfaces from rolling contact fatigue including wear, cracking, and micro-pitting.

Experimental

Lubricants

The base oil used for the experiments was a polyalphaolefin (PAO4) synthetic oil, with a reported kinematic viscosity of 4 cSt at 100°C, along with a 5 wt.% alkylated naphthalene (AN) co-solvent (ExxonMobil Chemical Co., Spring, TX).

The commercially-available ZrO_2 nanocrystals were synthesized using a patented solvothermal technique [45-46] which yields single-crystal ZrO_2 nanocrystals (Pixelligent Technologies LLC, Baltimore, MD, PixClear PC14-10-L01). Their structure and size were found to be crystalline with a nearly uniform diameter of 5 nm [40-43]. To enhance their dispersibility in oil, the NC's surfaces are treated and capped (functionalized) with an organic ligand to improve their dispersion stability in oil. The NC's dispersion was prepared by adding to base stock, 1 wt.% of ZrO_2 NCs, using the same method described previously [40-41-47]. No other co-additives were added to the tested oil dispersions in order to investigate the intrinsic action of ZrO_2 NCs without the effects of co-additives. The dispersions are optically clear with no measurable aggregation [41-47], and stable for years.

Micro-pitting tests

All testing discussed in the current work was conducted on a PCS Instruments micro-pitting rig (MPR). This rig utilizes a three ring-on-roller splash-lubricated line contact to study bearing and gear failure modes at an accelerated rate. The three outer rings and a central roller are operated using two separate motors. Therefore, variable levels of slip, ranging from pure rolling to pure sliding, can be studied. Additionally, the load, contact temperature, rolling speed, and therefore lubricant film thickness can be controlled. The test specimens were composed of AISI 52100 through-hardened martensitic steel. The Rockwell C hardness of the rollers and rings were measured as 60 and 63 respectively. The central test roller is the specimen of interest for the current work; the roller is 12 mm in diameter and has a central 1 mm wide test track. An image of the roller is shown in Figure 1. Based on the geometry of the contact, the specific contact conditions, and the viscosity of the lubricant, the lubricant film thickness can be calculated for each test using the modified Dowson-Hamrock equation given in Eqn. 1.

$$h_{min} = 2.65 \cdot U^{0.7} \cdot G^{0.54} \cdot W^{-0.13} \cdot R_r \qquad \text{Eqn. 1}$$

Within this equation h_{min} is the minimum film thickness between the two contacting bodies, U is the dimensionless speed parameter, G is the dimensionless material parameter, W is the dimensionless load parameter, and Rr is the reduced radius which is determined by the size of the two bodies in contact. This lubricant film thickness can then be used in conjunction with the compound roughness of the two surfaces to define the specific film thickness lambda; this calculation is shown in Eqn. 2.

$$\lambda = \frac{h_{min}}{R_C} \qquad \text{Eqn. 2}$$

Within this equation, h_{min} is the minimum film thickness calculated in Eqn. 1, and R_c is the composite RMS roughness of the two contacting services. The specific testing parameters used for the experiments discussed in the current work are shown in Table 1. The methodology for selecting these three testing conditions for FIB/TEM analysis is as follows. Tests 1 and 2 are designed to investigate the effect of incorporating ZrO_2 into a representative gear contact; Tests 2 and 4 can be compared to understand differences in tribofilm morphology in the presence of slip; and Tests 2 and 3 are designed to investigate the surface damage of rollers and tribofilm morphology as function of test duration.

Experiment #	Load (N)	Maximum Contact Stress (GPa)	Lubricant	SRR (%)	Composite Roughness *Rc* (nm)	λ	Total Testing Time (Hours)
1	200	1.2	PAO 4	30	655	0.3	119
2	200	1.2	PAO 4 + 1 wt.% ZrO_2	30	651	0.3	119
3	200	1.2	PAO 4 + 1 wt.% ZrO_2	30	645	0.3	4
4	200	1.2	PAO 4 + 1 wt.% ZrO_2	0	292	0.6	24

Table 1: Summary of MPR testing conditions at 200 N applied load, 2 m/s rolling speed, and 70 °C

Optical microscopy

Micro-pitting and wear damage of roller and rig surfaces were assessed using a standard optical microscope in bright field mode Olympus, STM6. An optical interferometer was used to measure the evolution of the surface roughness before and after testing Bruker, ContourGT-K.

Ion beam milling

TEM cross-sectional samples on roller surfaces were prepared using FEI Strata 235 FIB-SEM focused ion beam (FIB) instrument. A transverse cut was performed on the worn surface to obtain a cross section approximately 100 nm thick. Platinum layers were previously deposited on the worn track to preserve the surface from nanomachining by Ga+ ion beam.

Analytical TEM

TEM observations were performed on a JEOL 2010F field emission gun operating with a 200 kV accelerating voltage equipped with energy dispersive spectroscopy (EDS) and equipped with GATAN Imaging Filter (GIF200).

Results

1) Micro-pitting rig (MPR) test results

1-1) Performance of ZrO_2 dispersion against wear and micro-pitting damage at 30% SRR

First, we discuss MPR tests carried out at 30% SRR to investigate the influence of adding ZrO_2 NCs to base stock on the evolution of wear and micro-pitting of roller surfaces. Representative optical micrographs showing the wear track of the roller used in Experiments 1 and 2 at numerous temporal points throughout testing are shown in Fig. 2. This figure clearly illustrates that the use of a lubricant containing 1% wt. ZrO_2 nanocrystals leads to the formation of a robust tribofilm as indicated by the blue-brown coloration of running track; the color is due to optical interference from the translucent ZrO_2 film.

Small surface pits can be seen in some of the images. These pits were far more prevalent in the PAO 4 case than in the PAO 4 +1% ZrO_2 case, with counts of 85 surface pits, and 40 surface pits respectively, over the entirety of the wear track. Additionally, the pits that were observed in the PAO 4 case were significantly larger than those observed in the PAO 4 + 1% ZrO_2. To illustrate this, optical microscopy measurements of the pitted area for the three largest spalls were taken. The three largest pits for the PAO 4 + 1% ZrO_2 had areas of approximately 7300, 6300, and 5900 μm^2, while the three largest pits within the PAO 4 had areas of 7400, 5000, and 3500 μm^2. The largest pit in the PAO was an order of magnitude larger than the largest pit when the ZrO_2 nanocrystals were included. These pits constitute regions where surface cracks have initiated and propagated through the near surface region, likely driven by 30% SRR used during testing. It is important to note that in this orientation, the roller is acting as the follower; thereby accelerating surface initiated rolling contact fatigue [6-48]. The hypothesis for this difference in number and size of surface-initiated pits will be discussed in detail later.

The wear characteristics of Experiments 1 and 2 were also quantified by taking measurements of the track width at four locations, each separated by 90 degrees from one another on the roller. These measurements were taken at five temporal points throughout the tests. The wear track widths were then converted to wear volumes based on the known geometry of the roller specimens. The results of this analysis are shown in Fig. 3. From this figure, it can be observed that the PAO 4 + 1% ZrO_2 resulted in significantly more polishing during the run-in period of the test, when compared to the PAO 4 sample. However, after this run-in period, the PAO 4 + 1% ZrO_2 showed no further observable wear between the 20h and 119h step, whereas the PAO 4 sample continued to wear during this period. The increased polishing observed within the run-in of the PAO 4 + 1% ZrO_2 sample is likely a primary driver in the

decreased surface pitting observed during this test. This is due to the fact that this formulation will lead to the removal of asperities that could interact leading to cracking. Moreover, once a fully developed tribofilm forms, it adequately protects the samples against any further wear damage, as indicated by the lack of wear observed between 20 and 119 hours for the PAO 4 + 1% ZrO_2 sample.

1-2) Behavior of ZrO_2 NCs at pure rolling conditions

In order to study the effect that surface shear and slip have on the ZrO_2 NC's ability to form a tribofilm, Experiment 4 utilized pure rolling conditions and stopped at different duration intervals up to 24h. Figure 4 shows the evolution of the roller's surface at different test intervals. A tribofilm formed at pure rolling conditions is visible by optical imaging as early as 15 min. of testing (143,000 cycles). As shown in Figure 5, this initial film is in a transient state of formation, as it does not cover the entirety of the surface. The film continues to grow over time, and becomes more uniform throughout the entirety of the 24 hour test (13.8 million cycles). These results confirm the ability of ZrO_2 NCs in base oil to rapidly form a tribofilm under MPR contact conditions regardless the SRR ratio (30% vs 0%). Unlike the other additives such as ZDDP [49], shear stress is not required for nucleating and growing ZrO_2 tribofilms.

2) TEM characterizations of roller surfaces

Three TEM lamellae were removed from the surface of rollers lubricated with dispersion containing the ZrO_2 NCs using FIB technique, as shown in Fig. 6. The TEM lamella extracted from Experiments 2 and 3 were compared to study the effect of testing time on tribofilm morphology. The lamellae extracted from Experiment 4 (pure rolling) can be compared to the aforementioned two tests to see the effect that slip and tractive forces have on the formation of the tribofilm.

Figure 7 shows TEM micrographs taken at different magnifications of the roller surface tested under 30% SRR for a duration of 4h (Experiment 3). These micrographs are representative of the entire examination of the cross-sectional lamellae via TEM. A tribofilm with a thickness of approximately 100 nm is observed on the surface of steel. The tribofilm has a sharp interface with the steel surface, indicating that polishing of the asperities occurred prior to the film growth, consistent with the optical microscopy, and also indicating a uniform and potentially well-adhered interface devoid of gaps. The subsurface (depth up to 500 nm from the surface) did not exhibit signs of fatigue damage except the presence of a small amount of delamination of the steel surface of approximately 10 nm depth and 100 nm length (Fig. 8) and the presence of regions with darker contrast (Fig. 7a and 7b). The darkened contrast is typical of plastically deformed metals with a high density of dislocations within the grains located under the sliding interface [50].

As clearly seen in Fig. 7c, the tribofilm exhibits a highly dense polycrystalline microstructure, free of voids and cracks. TEM-based EDS profiles and atomic quantification from spot analysis (Fig. 9) show that the tribofilm is composed mainly of zirconium (Zr) and oxygen (O). Moreover, the tribofilm is nearly free of

carbon, demonstrating that the organic capping agents have been largely removed, and that hydrocarbon species from the PAO have not been incorporated into the film.

To verify the integrity of the ZrO_2 tribofilm at longer term, a cross-sectional lamella extracted from a surface roller after 119 h of testing was examined. Fig. 10 revealed the presence of a tribofilm covering the steel surface, which is present along the entire cross-sectional sample. The tribofilm has similar characteristics to that of the roller after 4h of testing, which confirm the robustness and persistence of the formed tribofilm under pressure and shear stresses induced by the rolling-sliding contact up to 119 h of testing. However, as can be seen in Fig. 11, a portion of the near surface material was subjected to visible fatigue involving different damage features. Fig. 11c shows a zoomed-in part of Fig. 11a where a partially delaminated region of the steel is surrounded by the tribofilm. The partial delamination occurs in the longitudinal direction (perpendicular to the rolling direction), a few tens of nanometer from the near surface material. The ZrO_2 NCs have penetrated deep inside the crack underneath the partially delaminated region, as can be seen in Fig. 11 a and c, and in Fig. 12. This filling in may help in limiting the delamination process. Also, in Fig 11 b and c and the region in Fig 11 a between them, a bright band between the tribofilm and the steel substrate is seen, which may indicate delamination of the tribofilm itself from the steel. In Fig. 11 d, both the near surface material and the tribofilm (as indicated by the bright band in the brighter tribofilm region, which is a sign of reduced density or a gap in the material) seem to be undergoing cracking, induced by applied stresses. In addition, Fig. 11 e illustrates a possible location of steel detachment, as indicated by the sloped region leading up from the crack below, as if there had been a partial delamination followed by fracture of the overhanging portion of the steel. A subsurface crack is seen oriented at an angle of approximately 10° to the surface. This region may shed light on the pit formation process.

The pixel reconstruction of EDS chemical mapping (fig 13b) recorded on the region of the cross-section around a partially delaminated region reveals that the bright areas surrounding the delaminated steel layer visible in Fig. 13a are rich in manganese (Mn), sulfur (S) and chromium (Cr), in addition to the expected elements (Fe, O and Zr) detected from the steel delaminated layer and the ZrO_2 tribofilm. In order to verify if the different surface alterations taking place on the roller during the 119h of testing are related to an unusually high concentration of Mn, S and Cr, all of the cracked and partially delaminated areas observed within the TEM lamella were investigated by EDS. Figure 14 illustrates a typical EDS profile recorded across a crack covered by a tribofilm. As expected, the tribofilm is rich in Zr and O while the steel substrate is mainly composed of Fe. The inside crack appears to be rich in Mn and S elements as attested by the sudden increase of their concentrations through the EDS profile (Mn and S peaks). These results provide evidence that cracks in the steel are initiated preferentially at heterogeneous nucleation sites rich in Mn and S. Atomic quantification from EDS analyses recorded on the steel substrate and inside cracks as illustrated in Fig. 15 show that the concentration of both Mn and S in these sites is significantly higher than in steel and are in the order of respectively 9 % and 6% while their concentration did not exceed 0.5% in steel. This suggests that the cracking observed in the surface was due to the presence of near surface manganese sulfide inclusions. These are relatively common in AISI

52100 steel. We note that this can also occur by interaction of S-containing EP additives at high pressures with the steel [21]; however, no such additives are present in these experiments.

The surface roller tested at pure rolling condition (Experiment 4) was also analyzed in TEM. As seen in Fig. 16, a tribofilm of a thickness varying between 50 and 70 nm is covering the steel surface all along the TEM lamella. This tribofilm is found to have a slightly lower thickness compared to the ones obtained at SRR 30%. Furthermore, no damage was detected in the near subsurface up to 500 nm depth. This suggests that the ZrO_2 NCs can form a protective tribofilm regardless the SRR ratio, and that this tribofilm once formed maintain its integrity.

Discussion

The aim of this work was to investigate the effect of ZrO_2 NCs as lubricant additives on the fatigue and wear of surfaces under rolling-sliding contact conditions.

The results clearly demonstrate the beneficial effect of ZrO_2 NCs in limiting the propagation of micro-pitting when used as additives in base stock. TEM images and EDS analyses of the cross-sectional FIB samples confirmed the ability of ZrO_2 NCs to form protective and robust tribofilms of approximately 100 nm in thickness. The tribofilms exhibit dense and polycrystalline texture indicating a significant influence of compaction and sintering of ZrO_2 NCs under stress. They were also found to be composed mainly of Zr and O. A sharp interface is observed between the steel substrate and the tribofilm indicating a polishing effect of the asperities during the running in phase. The EDS profile shows that the content of iron (Fe) in the tribofilm increases when approaching the interface with steel. This suggests that some wear debris from the steel substrate generated during the running-in phase of the test could be involved in the nucleation process of ZrO_2 tribofilms. However, the shape of the EDS profile at the interface may also arise from the finite size of the beam (a few nanometers) and also affected by artifacts such as the tilt of lamellae, or waviness of the interface along the direction of the beam (such that the beam samples some of the substrate and the tribofilm when imaging close to the interface). Hence, further characterization such as the use of ToF SIMS to determine the composition of the tribofilm at the interface would better elucidate the role of wear debris in the nucleation process of the tribofilms.

These characteristics are found to be common to the tribofilms generated at both 0% and 30% SRR which highlight that shear stress is not necessary to the growth process of ZrO_2 tribofilms. Hence, the potential of ZrO_2 NCs to form protective tribofilms with similar characteristics in term of structure and composition despite the SRR is an advantage compared with ZDDP. Indeed, the growth mechanisms of S-P additives such as ZDDP have been extensively investigated in the literature and it has been shown that shear stress is essential to nucleate and grow tribofilms derived from ZDDP [49-51]. As well, the lubrication mechanisms of other NP additives were found to be governed by the shear stress such as for IF-MeS_2 (Me=Mo and W) NPs. Their film formation mechanism is based on an exfoliation process of their outer layers, which is found to be active only under the combined effect of pressure and shear stress [52-53].

TEM examinations of the near subsurface (> 500 nm) of the roller tested under pure rolling for 24h (Experiment 4, Fig. 16) confirmed the absence of any fatigue damage. Neither cracks nor micro-pits were observed. Under the more severe conditions (Experiment 3, 30% SRR), the near surface material of the roller tested for 4h (Fig. 7-9) has only limited plastic deformation and/or microstructural distortion, although, as only one example of delamination of steel was observed in the lamella (Fig. 8). Moreover, the presence of ZrO_2 tribofilm around it suggests the ZrO_2 may have helped stop its propagation. Furthermore, the sharp interface between steel surface and the formed tribofilm suggests a polishing effect of asperities prior to the growth of the tribofilm. Such wear may be beneficial, because it leads to a smoothing of the rough counter-face resulting in less stress concentrations.

For the longer-term test of 119h at 30% SRR (Experiment 2), the TEM results confirm the presence of ZrO_2 tribofilm with a thickness varying between 30 nm and 100 nm, and with similar structure and composition as the one observed after 4h of testing. This suggests that the tribofilm, once formed, maintains a consistent morphology in the presence of cyclic stresses. This idea is consistent with *in-situ* measurements of ZrO_2 tribofilm growth in PAO and other lubricants via AFM [40-41-42] where films progressively grow until they reach their maximum thickness, at which point the height fluctuates modestly as sliding proceeds. We note that mini-traction machine (MTM) experiments with *in-situ* spacer layer imaging (SLIM) thickness measurements have indicated some amount of removal as the film first forms, but then the thickness stabilizes [44-47-54].

Nevertheless, some regions of the tribofilm exhibit localized damage features such as delaminated layers and cracks (Fig. 11). These damage features exist close to the surface with a depth in the range of 20 nm to 200 nm, and an angle to the surface between 0° and 10°. They are surrounded by the ZrO_2 tribofilm at their upper side (Fig. 13, 14, and 15), and their inside is filled with ZrO_2 NCs (Fig. 12); the contrast of this ZrO_2-containing region is different from the tribofilm, indicating that it is composed of individual NC's that have not been sintered (or are only partially sintered) due to being subject to less contact pressure for less time than the tribofilm. They may be initiated mainly under the action of shear (Fig. 11d), as suggested by their longitudinal orientation. This may be explained by the fact that ZrO_2 tribofilms did not provide enough relaxation of the contact shear stresses, due to their high mechanical hardness and modulus [41]. The addition of an effective friction modifier additive to the ZrO_2 dispersion may improve micro-pitting through reducing friction and shear stress, which can likely reduce crack opening and propagation. For example, Lainé et al. [55] have shown that the micro-pitting damage encountered with ZDDP can be greatly reduced when the friction modifier MoDTC is also present. They suggest that the observed improvement is attributed to the reduced asperity friction by a mechanism involving local deposition of MoS_2 leading to lower tensile stresses and an increase in critical crack size for propagation. This may be a worthy topic for future study.

EDS analyses revealed an unexpected high concentration of Mn and S close to the cracks and delaminated areas (Fig. 13-14-15). This high concentration was systematically observed close to all of the damage features existing on the TEM lamella of the roller tested at SRR30% for a duration of 119h

(Experiment 2), demonstrating that the initiation of subsurface damage was directly connected with heterogeneous sites in steel. Surveying the literature, it has been reported that MnS inclusions in steel can act as crack initiation sites under high enough contact stress [56-57-58-59]. It has been found that during quenching of bearing steel, the different thermal contraction rates of the bulk material and MnS inclusions may weaken the bond between the inclusion and the surrounding bulk material, or possibly lead to the creation of free surface at the inclusion/steel boundary [50]. These free surfaces are potential sites for inclusion separation from the bulk material and for initiating cracking under cyclic loading [60-61]. Furthermore, even thin and flattened MnS inclusions may act as stress concentrators that may initiate cracks [62]. Considering that the damage features were localized near the surface of steel (in the range of 10 nm to 200 nm) (Fig. 11), it appears that MnS inclusions were present near the roller's surface. Hence, a possible scenario for the crack/delamination shown for example in Fig. 13 could be related to the presence of a MnS inclusion towards the end of the crack tip, possibly located in the region denoted by the dashed oval. This inclusion could have acted as a stress concentrator that initiated the crack itself. Once the crack interacted with the inclusion, it allowed for the inclusion to deform as MnS inclusions are relatively soft, and be transported into the lubricant during the test. As the inclusion escapes it is sheared across the crack faces, leaving a MnS-rich coating on the entire inside of the crack face. The ZrO_2 then filled the void left by the inclusion as can be seen in Fig. 13. Recent work has shown that Mn has a strong affinity for the ZrO_2 surface, and this may further promote stress-assisted transport of Mn along the steel-ZrO_2 interface [63]. Another argument to explain the high concentration of Mn and S elements within the face of cracks is that these two elements diffusively migrated from the steel itself to the crack tip due to crack face rubbing and subsequent energy localization. This hypothesis is almost certainly energetically impossible, given that the diffusion of these two elements in steel is extremely difficult. It was estimated that it would take weeks at temperatures of over 400°C to get these elements to migrate from the surrounding regions [64]. Moreover, the amount of Mn and S within the steel (not precipitated as inclusions) is extremely small; therefore, the atomic levels given within the TEM-EDS analysis (Fig. 15) almost certainly require the presence of an inclusion. Finally, we consider the possible impact of FIB processing, where an inclusion could be milled away during the last steps of thinning that distributed the atoms of the inclusion to surrounded region. While possible, this is unlikely since, if this was the case, Mn and S elements would be distributed across the entirety of the tribofilm, as opposed to concentration in the crack tip as confirmed the EDS results. These results shed the light on the role of the inclusions and more generally the microstructure of steel on the fatigue damage of surfaces under rolling-sliding cyclic contact.

Conclusion

In summary, the role of ZrO_2 NCs in LV base stock in preventing surfaces tested under rolling-sliding contact conditions from fatigue damage and wear was investigated using a micro-pitting rig. FIB sample preparation and TEM techniques were used to analyze the surface of rollers lubricated with a 1 wt.% ZrO_2 dispersion and tested at two different levels of SRR (30% and 0%) and at different test durations (4h, 24h

and 119h) under a maximum Hertzian stress of 1.2 GPa. The major conclusions of this work were as follows:

- The LV base stock containing 1 wt.% ZrO_2 provides a protection against surface fatigue through a two-step mechanism. During the running-in phase, ZrO_2 NCs contribute to increase the wear rate in comparison with the PAO4, which results in an accelerated asperity polishing and therefore, potentially a mitigation of the initiation of surface cracks. Then, during the steady state phase, between 20h and 119h, no observable wear occurred while the surfaces lubricated with PAO4 continued to wear, attributed to the presence of the ZrO_2 tribofilm protecting the surfaces from wear.

- The roller surface lubricated with PAO4 + 1 wt. % ZrO_2 showed significantly fewer and smaller pits in comparison with rollers lubricated with PAO4. This is attributed to the combined effect of decreasing the severity of the contact through tribofilm growth and the ingress of NCs into the surface cracks.

- ZrO_2 NCs form dense, tribo-sintered surface-bound tribofilms regardless the rolling-sliding ratio and the testing duration.

- Evidence suggests that the initiation of cracks is directly connected with the presence of heterogeneous MnS inclusions in standard AISI 52100 steel which highlights the impact of the microstructure of tribo-pair surfaces on their longevity.

Declarations

Acknowledgement

This material is based upon work supported by the U.S. Department of Energy, Office of Science, under the Small Business Innovation Research (SBIR) and Small Business Technology Transfer Program SBIR-II Award Number DE-SC-0009222, and under the Advanced Manufacturing Office Award Number DE-EE0009120.

I.L. acknowledges support from an Africk Fellowship from the University of Pennsylvania.

This work was carried out in part at the Singh Center for Nanotechnology, which is supported by the NSF National Nanotechnology Coordinated Infrastructure Program under grant NNCI-2025608.

We thank Dr. H. Khare for useful discussions.

References

[1] Fontaras, G., Vouitsis, E., and Samaras, Z.: Experimental Evaluation of the Fuel Consumption and Emissions Reduction Potential of Low Viscosity Lubricants. SAE Technical Paper (2009). https://doi.org/10.4271/2009-01-1803.

[2] Zhou, R.S., Cheng, H. S., Mura, T.: Micropitting in Rolling and Sliding Contact Under Mixed Lubrication. *J. Tribol*. (1989). https://doi.org/10.1115/1.3261984

[3] Evans, M.-H.: An updated review: white etching cracks (WECs) and axial cracks in wind turbine gearbox bearings. Mater. Sci. Technol. (2016). https://doi.org/10.1080/02670836.2015.1133022

[4] Vrcek, A., Hultqvist, T., Baubet, Y., Björling, M., Marklund, P., Larsson, R.: Micro-Pitting and Wear Assessment of PAO vs Mineral-Based Engine Oil Operating under Mixed Lubrication Conditions: Effects of Lambda, Roughness Lay and Sliding Direction. Lubricants (2019). https://doi.org/10.3390/lubricants7050042

[5] Morales-Espejel, G.E., Rycerz, P., Kadiric, A. : Prediction of micropitting damage in gear teeth contacts considering the concurrent effects of surface fatigue and mild wear. Wear (2018). https://doi.org/10.1016/j.wear.2017.11.016

[6] Gould, B., Greco, A.: The Influence of Sliding and Contact Severity on the Generation of White Etching Cracks. Tribol Lett. (2015). https://doi.org/10.1007/s11249-015-0602-6

[7] Rycerz, P., Kadiric, A.: The Influence of Slide–Roll Ratio on the Extent of Micropitting Damage in Rolling–Sliding Contacts Pertinent to Gear Applications. Tribol. Lett. (2019). https://doi.org/10.1007/s11249-019-1174-7

[8] Cen, H., Morina, A., Neville, A.: Effect of slide to roll ratio on the micropitting behavior in rolling-sliding contacts lubricated with ZDDP-containing lubricants. Tribol. Int. (2018). https://doi.org/10.1016/j.triboint.2018.02.038

[9] Mayeur, C., Sainsot, P., and Flamand, L.: A Numerical Elastoplastic Model for Rough Contact. ASME. *J. Tribol*. (1995). https://doi.org/10.1115/1.2831270

[10] Ye Zhou, Caichao Zhu, Benjamin Gould, Nicholaos G. Demas, Huaiju Liu, Aaron C. Greco. The effect of contact severity on micropitting: Simulation and experiments. Tribol. Int. (2019). https://doi.org/10.1016/j.triboint.2019.06.020

[11] Evans, R. D., Doll, G. L. ., Hager, C. H., Howe, J. Y.: Influence of Steel Type on the Propensity for Tribochemical Wear in Boundary Lubrication with a Wind Turbine Gear Oil. Tribol Lett (2010). https://doi.org/10.1007/s11249-009-9565-9

[12] Bruce, T., Long, H., Slatter, T., Dwyer-Joyce, R. S.: Formation of white etching cracks at manganese sulfide (MnS) inclusions in bearing steel due to hammering impact loading. Wind Energy (2016). https://doi.org/10.1002/we.1958

[13] Gould, B., Paladugu, M., Demas, N.G., Greco, A.C.: Figure the impact of steel microstructure and heat treatment on the formation of white etching cracks. Tribol. Int. (2019). https://doi.org/10.1016/j.triboint.2019.02.003

[14] Gould, B., Demas, N.G., Pollard, G., Rydel, J.J., Ingram, M., Greco, A.C.: The effect of lubricant composition on white etching crack failures. Tribol. Lett. (2019). https://doi.org/10.1007/s11249-018-1106-y

[15] de la Guerra Ochoa, E., Echávarri Otero, J., Chacón Tanarro, V., Munoz-Guijosa, J.M. ., del Río López, B., Cordero, C.A.: Analysis of the effect of different types of additives added to a low viscosity polyalphaolefin base on micropitting. Wear (2015). https://doi.org/10.1016/j.wear.2014.11.014.

[16] Lainé, E., Olver, A.V., Beveridge, T.A.: Effect of lubricants on micropitting and wear. Tribol. Int. (2008). https://doi.org/10.1016/j.triboint.2008.03.016

[17] Vrbka, M., Šamánek, O., Šperka, V., Návrat, T., Křupka, I., Hartl, M.: Effect of surface texturing on rolling contact fatigue within mixed lubricated non-conformal rolling/sliding contacts. Tribol. Int. (2010). https://doi.org/10.1016/j.triboint.2010.02.002

[18] Brechot, P., Cardis, A.B., Murphy, W.R. and Theissen, J.: Micropitting resistant industrial gear oils with balanced performance. Ind. Lubr. Tribol. (2000). https://doi.org/10.1108/00368790010371762

[19] Evans, R.D., Nixon, H.P., Darragh, C.V., Howe, J.Y., Coffey, D.W.: Effects of extreme pressure additive chemistry on rolling element bearing surface durability. Tribol. Int. (2007). https://doi.org/10.1016/j.triboint.2007.01.012

[20] Paladugu, M., Lucas, D.R., Scott Hyde, R.: Effect of lubricants on bearing damage in rolling-sliding conditions: Evolution of white etching cracks. Wear (2018). https://doi.org/10.1016/j.wear.2017.12.001.

[21] L'Hostis, B., Minfray, C., Frégonèse, M., Verdu, C., Ter-Ovanessian, B., Vacher, B., Le Mogne, T., Jarnias, F., Da-Costa D'Ambros, A.: Influence of lubricant formulation on rolling contact fatigue of gears – interaction of lubricant additives with fatigue cracks. Wear (2017). https://doi.org/10.1016/j.wear.2017.04.025

[22] Evans, R.D., More, K.L., Darragh, C.V., Nixon, H.P.: Transmission Electron Microscopy of Boundary-Lubricated Bearing Surfaces. Part I: Mineral Oil Lubricant, Tribol. Trans. (2004). https://doi.org/10.1080/05698190490463286

[23] Evans, R.D., More, K.L., Darragh, C.V., Nixon, H.P.: Transmission Electron Microscopy of Boundary-Lubricated Bearing Surfaces. Part II: Mineral Oil Lubricant with Sulfur-and Phosphorus-Containing Gear Oil Additives, Tribol. Trans. (2005). https://doi.org/10.1080/05698190590965602

[24] Gosvami, N. N., Bares, J. A., Mangolini, F., Konicek, A. R., Yablon, D. G., Carpick, R. W.: Mechanisms of antiwear tribofilm growth revealed in situ by single-asperity sliding contacts.

Science (2015). https://doi.org/10.1126/science.1258788

[25] Gosvami, N.N., Lahouij, I, Ma, J. Carpick, R.W.: Nanoscale in situ study of ZDDP tribofilm growth at aluminum-based interfaces using atomic force microscopy, Tribol. Inter. (2020). https://doi.org/10.1016/j.triboint.2019.106075.

[26] Meheux, M., Minfray, C., Ville, F., Le Mogne, T., Lubrecht, A.A., Martin, J.M., Lieurade, H.P., Thoquenne, G.: Effect of lubricant additives in rolling contact fatigue. Proc. IMechE Vol. 224 Part J: J. Engineering Tribology (2010). https://doi.org/10.1243/13506501JET719

[27] Benyajati, C., Olver, A.V., Hamer, C.J.: An experimental study of micropitting, using a new miniature test-rig. Tribol. Ser. (2003). https://doi.org/10.1016/S0167-8922(03)80088-3

[28] Brizmer, V., Pasaribu, H. R., Morales-Espejel, G. E.: Micropitting Performance of Oil Additives in Lubricated Rolling Contacts. Tribol. Trans. (2013). https://doi.org/10.1080/10402004.2013.790097

[29] Torrance, A.A., Morgan, J.E., Wan, G.T.Y.: An additive's influence on the pitting and wear of ball bearing steel. Wear (1996). https://doi.org/10.1016/0043-1648(95)06751-5

[30] Benyajati, C., Olver, A.V.: The effect of a ZnDTP anti-wear additive on micropitting resistance of carburised steel rollers. AGMA Tech Pap, pp.1–10 (2004)

[31] Tuszynnski, W., and Piekoszewski, W.: Effect of the Type and Concentration of Lubricating Additives on the Antiwear and Extreme Pressure Properties and Rolling Fatigue Life of a Four-Ball Tribosystem. Lubrication Science (2006). https://doi.org/10.1002/ls.25

[32] Ueda, M., Spikes, H., Kadiric, A.: *In-situ* observations of the effect of the ZDDP tribofilm growth on micropitting. Tribol. Int. (2019). https://doi.org/10.1016/j.triboint.2019.06.007

[33] Lahouij, I., Vacher, B., Martin, J. M., Dassenoy, F.: IF-MoS_2 Based Lubricants: Influence of Size, Shape and Crystal Structure, Wear (2012). https://doi.org/10.1016/j.wear.2012.07.016

[34] Sgroi, M., Gili, F., Lahouij, I., Dassenoy, F.: Friction Reduction Benefits in Valve-Train System Using IF-MoS_2 Added Engine Oil. Tribol. Trans. (2014). https://doi.org/10.1080/10402004.2014.960540

[35] Tannous, J., Dassenoy, F., Lahouij, I., Le Mogne, T., Vacher, B., Bruhács, A., Tremel, W.: Understanding the Tribochemical Mechanisms of IF-MoS_2 Nanoparticles Under Boundary Lubrication. Tribol. Lett. (2011). https://doi.org/10.1007/s11249-010-9678-1

[36] Chen, Y., Renner, P., Liang, H.: Dispersion of Nanoparticles in Lubricating Oil: A Critical Review. Lubricants (2019). https://doi.org/10.3390/lubricants7010007

[37] Fernández Rico, E., Minondo, I., García Cuervo, D.: Rolling contact fatigue life of AISI 52100 steel balls with mineral and synthetic polyester lubricants with PTFE nanoparticle powder as an additive. Wear (2009). https://doi.org/10.1016/j.wear.2008.08.020

[38] Ussa Aldana, P., Dassenoy, F., Vacher, B., Le Mogne, T., Thiebaut, B., Bouffet, A.: Antispalling Effect of WS_2 Nanoparticles on the Lubrication of Automotive Gearboxes. Tribology Transaction. (2016). https://doi.org/10.1080/10402004.2015.1061080

[39] Roy, S., Jazaa, Y., Sundararajan, S.: Investigating the micropitting and wear performance of copper oxide and tungsten carbide nanofluids under boundary lubrication. Wear (2019). https://doi.org/10.1016/j.wear.2019.03.007

[40] Lahouij, I., Carpick, R.W., Jackson, A., Khare, H.S., Gosvami, N.N., Demas, N.G., Greco, A.C., Fenske, G.R., Xu, W., Cooper, G., Chen, Z.: Nano-additives enabled advanced lubricants. US Patent App. US 2018 / 0127676 A1

[41] Khare, H.S., Lahouij, I., Jackson, A., Feng, G., Chen, Z., Cooper, G.D., Carpick, R.W.: Nanoscale generation of robust solid films from liquid-dispersed nanoparticles via *in situ* atomic force microscopy: growth kinetics and nanomechanical properties. ACS Appl. Mater. Inter. (2018). https://doi.org/10.1021/acsami.8b16680

[42] Khare, H.S., Gosvami, N.N., Lahouj, I., Milne, Z.B., McClimon, J.B., Carpick, R.W.: Nanotribological printing: a nanoscale additive manufacturing method. Nano Lett. (2018). https://doi.org/10.1021/acs.nanolett.8b02505

[43] Elinski, M.B., LaMascus, P., Zheng, L., Jackson, A., Wiacek, R.J., Carpick, R.W.: Cooperativity Between Zirconium Dioxide Nanoparticles and Extreme Pressure Additives in Forming Protective Tribofilms: Toward Enabling Low Viscosity Lubricants. Tribol. Lett. (2020). https://doi.org/10.1007/s11249-020-01346-1

[44] Thrush, S.J., Comfort, A.S., Dusenbury, J.S., Han, X., Wang, X., Qu, H., Barber, G.C.: Study of pressure dependence on sinterable zirconia nanoparticle tribofilm growth. Tribol.Inter. (2021). https://doi.org/10.1016/j.triboint.2020.106683.

[45] Williams, Z.S.G., Wang, Y., Wiacek, R.J., Bai, X., Gou, L.,Thomas, S.I., Xu, W., and Xu, J.: Synthesis, capping and dispersion of nanocrystals. WO/2011/133228 (2011).

[46] Williams, Z.S.G., Wang, Y., Wiacek, R.J., Bai, X., Gou, L., Thomas, S.I., Xu, W., and Xu, J.: Synthesis, capping and dispersion of nanocrystals. WO/2012/058271 (2012).

[47] Thrush, S.J., Comfort, A.S., Dusenbury, J.S., Xiong, Y., Qu, H., Han, X., Schall, J.D., Barber, G.C., Wang, X.:Stability, Thermal Conductivity, Viscosity, and Tribological Characterization of Zirconia Nanofluids as a Function of Nanoparticle Concentration. Tribology Transaction (2019).

DOI: 10.1080/10402004.2019.1660017

[48] Spikes, H.A., Olver, A.V., Macpherson, P. B.: Wear in rolling contacts. Wear (1986). https://doi.org/10.1016/0043-1648(86)90236-X

[49] Zhang, J., Spikes, H.: On the mechanism of ZDDP antiwear film formation. Tribol. Lett. (2016).

https://doi.org/10.1007/s11249-016-0706-7

[50] Williams, D.B., Carter, C.B.: Transmission electron microscopy: a textbook for materials science. 2nd ed. New York: Springer; 2009. https://doi.org/10.1007/978-0-387-76501-3

[51] Gauvin, M., Dassenoy, D., Minfray, C., Martin, J.M., Montagnac, G., Reynard, B.: Zinc phosphate chain length study under high hydrostatic pressure by Raman spectroscopy.

J.A.P. (2007). https://doi.org/10.1063/1.2710431

[52] Lahouij, I., Dassenoy, F., Vacher, B., Martin, J. M.: Real Time TEM Imaging of Compression and Shear of Single Fullerene-Like MoS2 Nanoparticle. Tribol Lett. (2012). https://doi.org/10.1007/s11249-011-9873-8

[53] Lahouij, I., Vacher, B., Dassenoy, F.: Direct observation by in situ transmission electron microscopy of the behaviour of IF-MoS2 nanoparticles during sliding tests: influence of the crystal structure. Lubrication Science (2013). https://doi.org/10.1002/ls.1241

[54] Thrush, S.J., Comfort, A.S., Dusenbury, J.S., Han, X., Barber, G.C., Wang, X., Qu, H.: Wear mechanisms of a sintered tribofilm in boundary lubrication regime. Wear (2021). (https://doi.org/10.1016/j.wear.2021.203932

[55] Lainé, E., Olver, A. V., Lekstrom, M. F., Shollock, B. A., Beveridge, T. A., Hua, D. Y.: The Effect of a Friction Modifier Additive on Micropitting. Tribol. Trans. (2009). https://doi.org/10.1080/10402000902745507

[56] Gould, B, Demas, N.G., Greco, A.C.: The influence of steel microstructure and inclusion characteristics on the formation of premature bearing failures with microstructural alterations. Mat. Sci. Eng. (2019). https://doi.org/10.1016/j.msea.2019.02.084

[57] Gould, B., Greco, A.C., Stadler, K., Vegter, E., Xiao, X.: Using advanced tomography techniques to investigate the development of White Etching Cracks in a prematurely failed field bearing. Tribol. Int. (2017). https://doi.org/10.1016/j.triboint.2017.07.028

[58] Gould, B., Greco, A.C., Stadler, K., Xiao, X.: An analysis of premature cracking associated with microstructural alterations in an AISI 52100 failed wind turbine bearing using X-ray tomography. Mater. Des. (2017). https://doi.org/10.1016/j.matdes.2016.12.089

[59] Costa e Silva, A.L.V.d.: The effects of non-metallic inclusions on properties relevant to the performance of steel in structural and mechanical applications. J. Mater. (2019). https://doi.org/10.1016/j.jmrt.2019.01.009.

[60] Sabirov, I., Kolednik, O.: The effect of inclusion size on the local conditions for void nucleation near a crack tip in a mild steel. Scr. Mater. (2005). https://doi.org/10.1016/j.scriptamat.2005.08.027

[61] Maciejewski, J.: The Effects of Sulfide Inclusions on Mechanical Properties and Failures of Steel Components. J Fail. Anal. and Preven. (2015). https://doi.org/10.1007/s11668-015-9940-9

[62] Schäfer, B.J., Sonnweber-Ribic, P., ul Hassan, H., Hartmaier, A.: Micromechanical Modeling of Fatigue Crack Nucleation around Non-Metallic Inclusions in Martensitic High-Strength Steels. Metals (2019). https://doi.org/10.3390/met9121258

[63] Li, Y., Wan, X.L., Cheng, L., Wu, K.M.: First-principles calculation of the interaction of Mn with ZrO2 and its effect on the formation of ferrite in high-strength low-alloy steels. Scr Mater. (2014). https://doi.org/10.1016/j.scriptamat.2013.11.028

[64] Dhua, S.K., Ray, A., Sen, S.K., Prasad, M.S., Mishra, K.B., Jha, S.: Influence of nonmetallic inclusion characteristics on the mechanical properties of rail steel. J. of Materi Eng and Perform. (2000). https://doi.org/10.1361/105994900770345584

Figures

Figure 1

Micro-pitting rig (MPR) test chamber, image of test specimens (disc and roller) showing the contact region

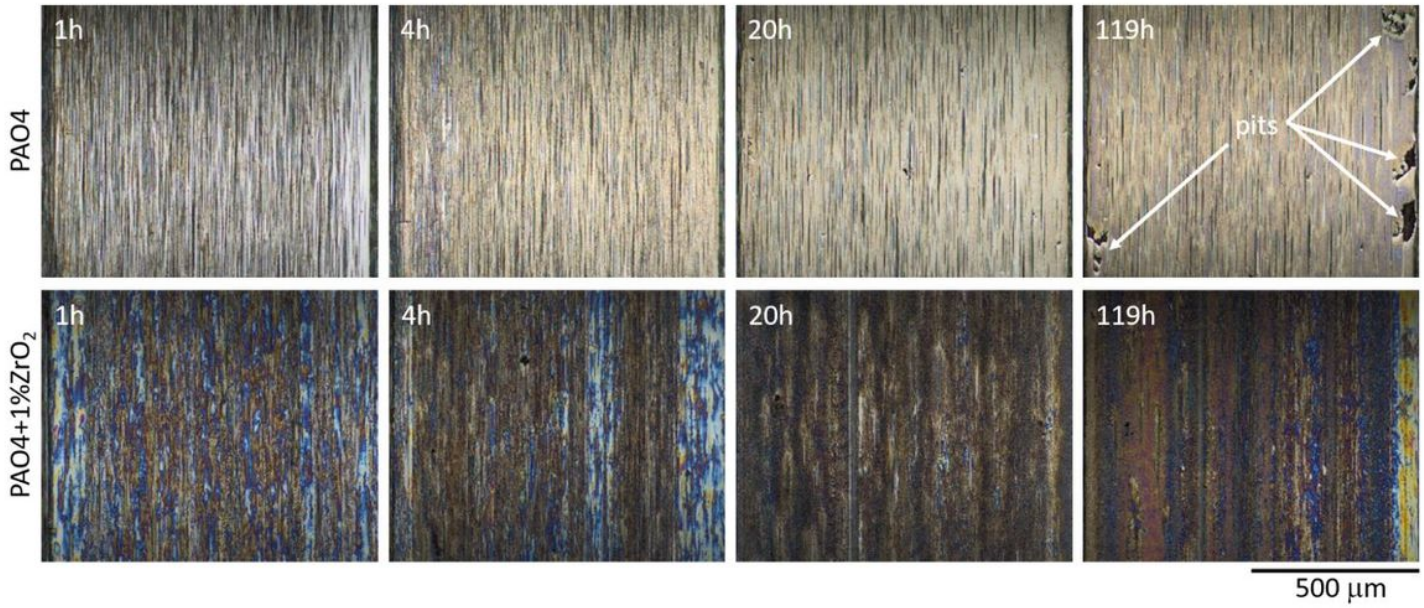

Figure 2

Optical micrographs of roller surfaces tested at 30% SRR and lubricated with PAO4 (top row, from Experiment 1) and PAO4+1% ZrO2 (bottom row, from Experiment 2) at 1h, 4h, 20h and 119h of testing respectively. In the ZrO2 lubricated contact, cracks and pits did not propagate and in some cases, they were recovered, while in PAO4 lubricated contact, cracks and pits that propagate were observed. The rolling direction in the images is top to bottom, and the images are not taken at the same location of the wear track.

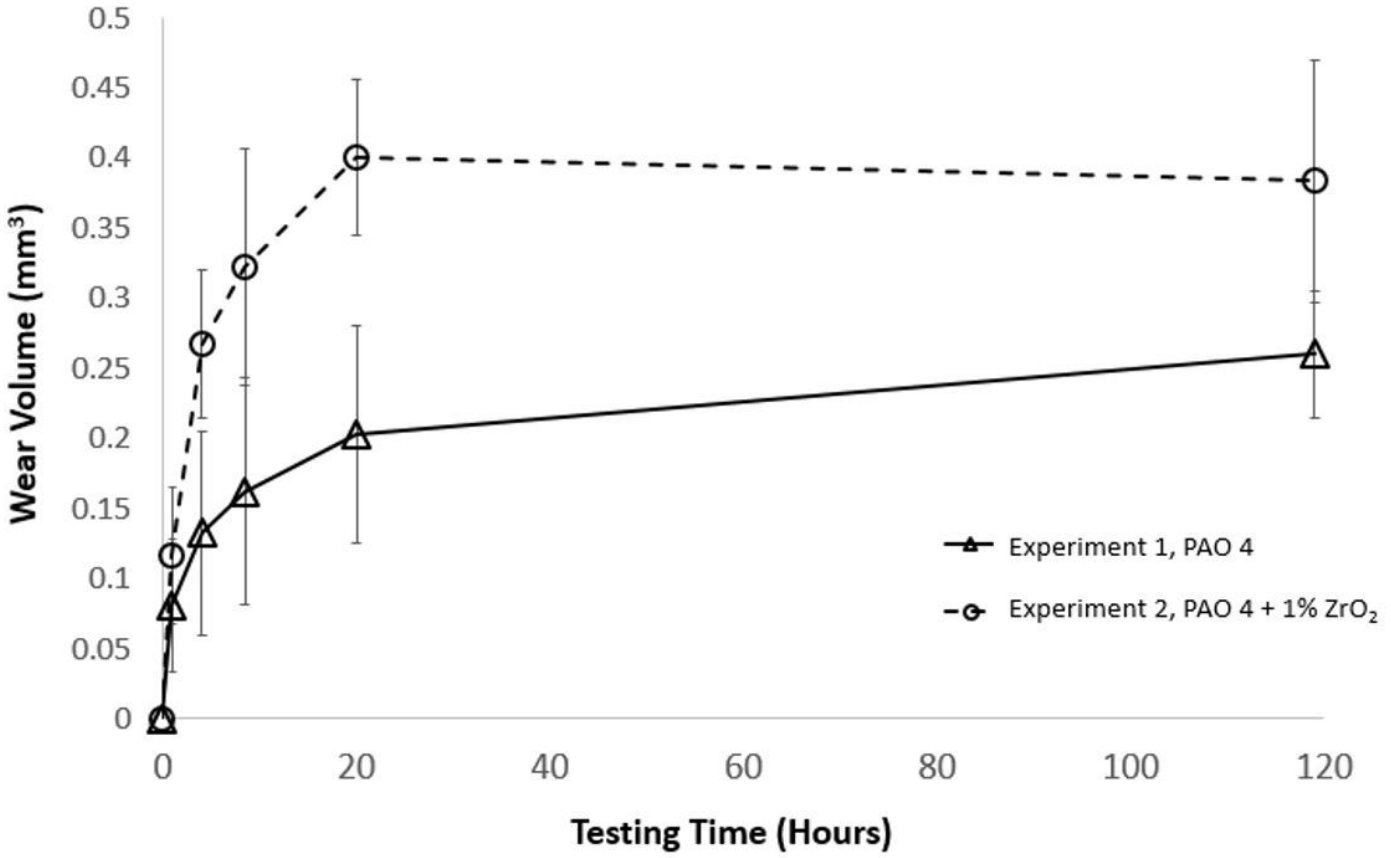

Figure 3

The wear characteristics of Experiments 1 and 2, which utilized identical running conditions to study the effect of incorporating 1% wt. ZrO2 NCs into PAO 4 base oil. The lubricant containing the nanocrystals runs in at an accelerated rate, resulting in polishing and potentially mitigating the initiation of surface cracks. After this initial run-in period, the sample was adequately protected by the tribofilm and the wear halted.

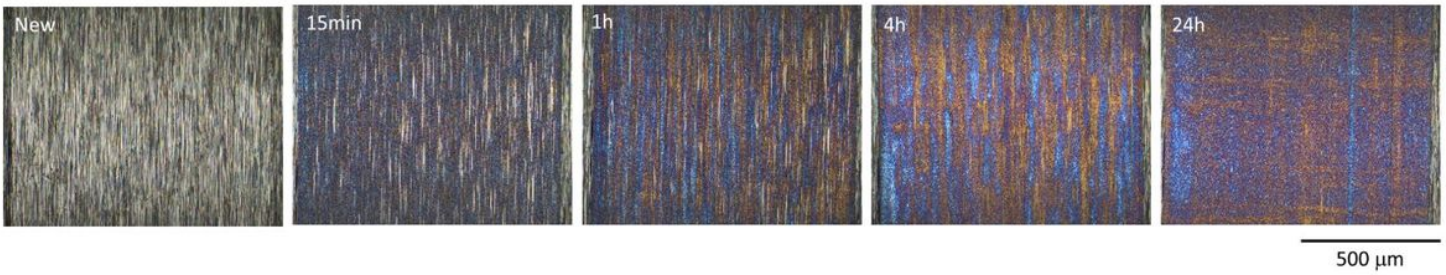

Figure 4

Optical micrographs of roller surfaces tested at pure rolling and lubricated PAO4+1% ZrO2, from Experiment 4. The observations were made before testing and after 15min, 1h, 4h, and 24h of testing. Rolling direction: top to bottom. After 15 min. of testing, the machining grooves (from the original

roughness of the specimen) start to disappear, leading to the formation of a tribofilm (brown and blue spots)

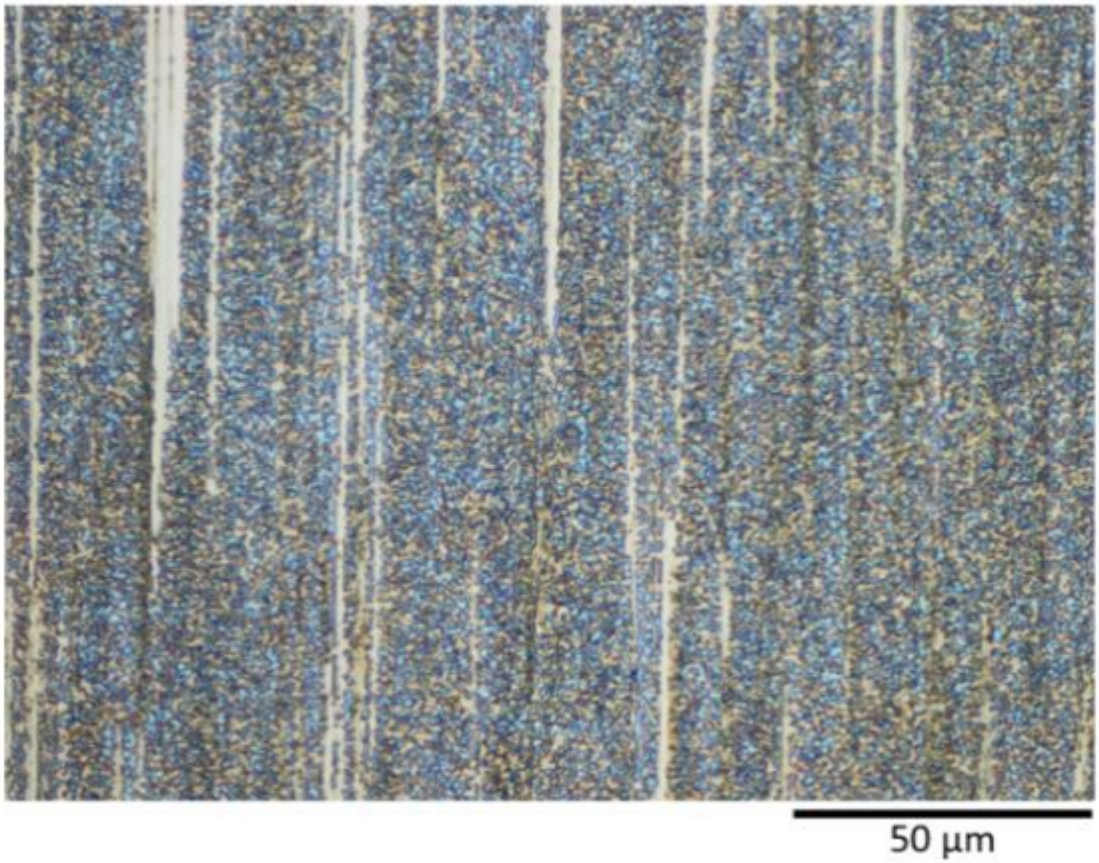

Figure 5

Zoom in on the surface contact region of the roller from Experiment 4 (PAO4 + 1 wt.% ZrO2) after 15 min. of testing, highlighting the formation of a tribofilm (indicated by the presence of brown and blue regions).

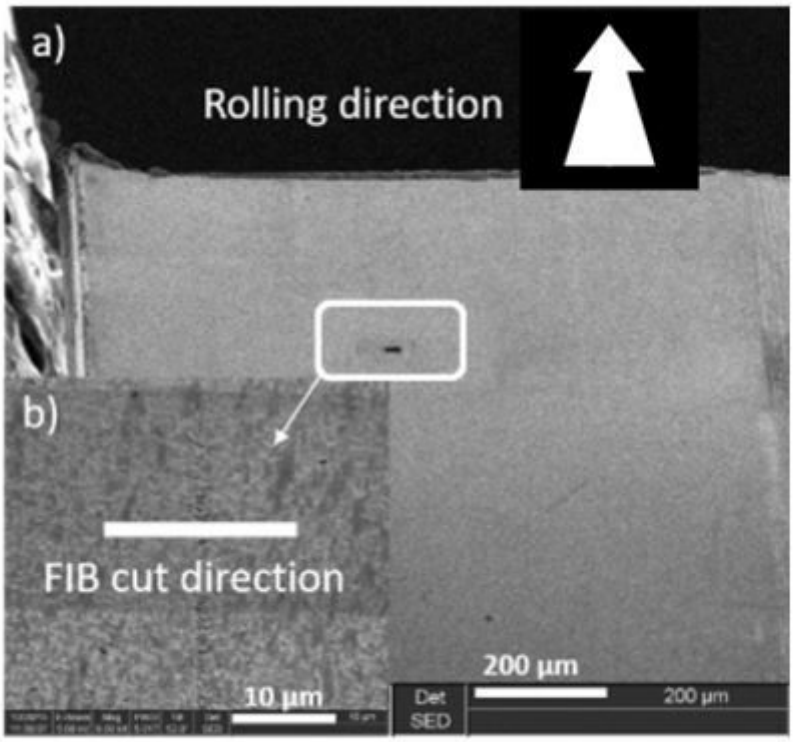

Figure 6

a) SEM micrograph of the lamella extracted from Experiment 3, which is representative of each of the lamellae extracted. The rolling direction is into the plane of the image. b) Zoom in of a), indicating the orientation of FIB cut.

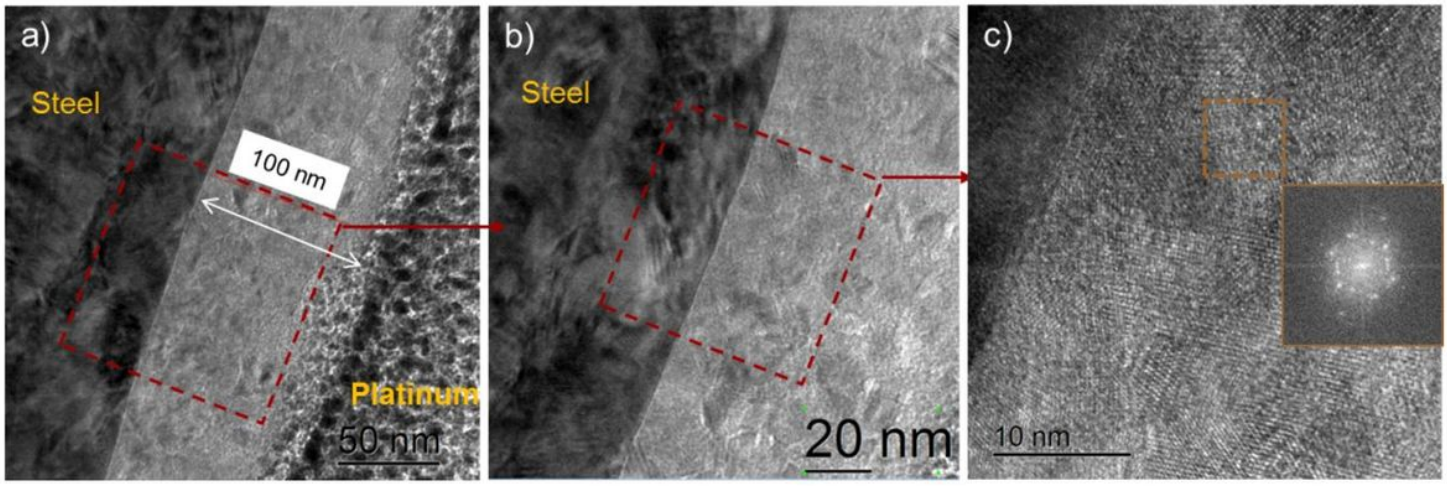

Figure 7

Cross sectional TEM micrographs of a roller surface lubricated with PAO4+1% ZrO2 at 30% SRR after 4h of testing (Experiment 3). (a) Overview showing a continuous and thick tribofilm (100 nm), note that the platinum is deposited to protect the tribofilm from ion milling. (b) Zoom in of the red box on (a) showing

a polished and sharp interface between steel and tribofilm suggesting the polishing of asperities prior to film formation. (c) High resolution TEM image and Two-dimensional fast Fourier transform (FFT) analysis showing the dense and crystalline structure of ZrO2 tribofilm.

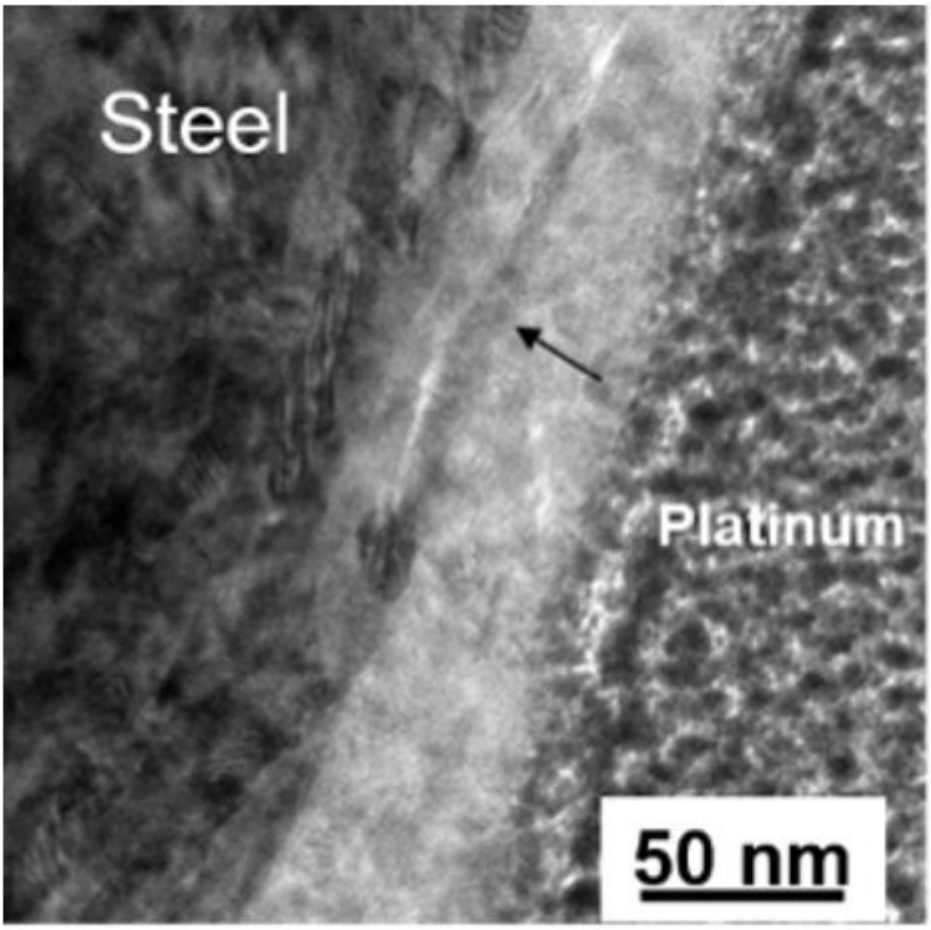

Figure 8

Cross sectional TEM micrograph of a roller surface lubricated with PAO4+1% ZrO2 at 30% SRR after 4h of testing (Experiment 3) showing the presence of a small longitudinal delamination of the steel surface of 10 nm depth. The inside crack is filled with the tribofilm. Note that no other cracks were observed in the lamella.

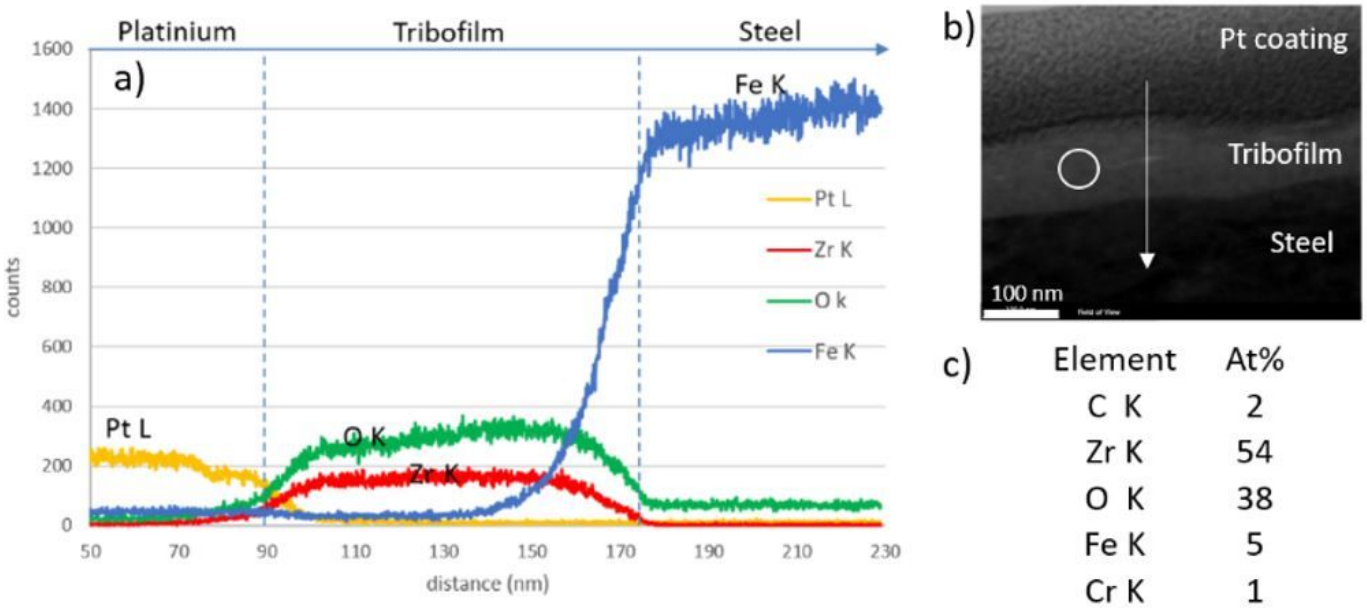

Figure 9

(a) EDS profile showing the relative content of oxygen, zirconium, iron and platinum within the TEM cross-section depth of the PAO4+1% ZrO2 at 30% SRR after 4h of testing (Experiment 3). (b) STEM micrograph indicating the line scan of the profile, and the location selected for spot analysis. (c) Table showing atomic quantification of the tribofilm composition from the spot analysis.

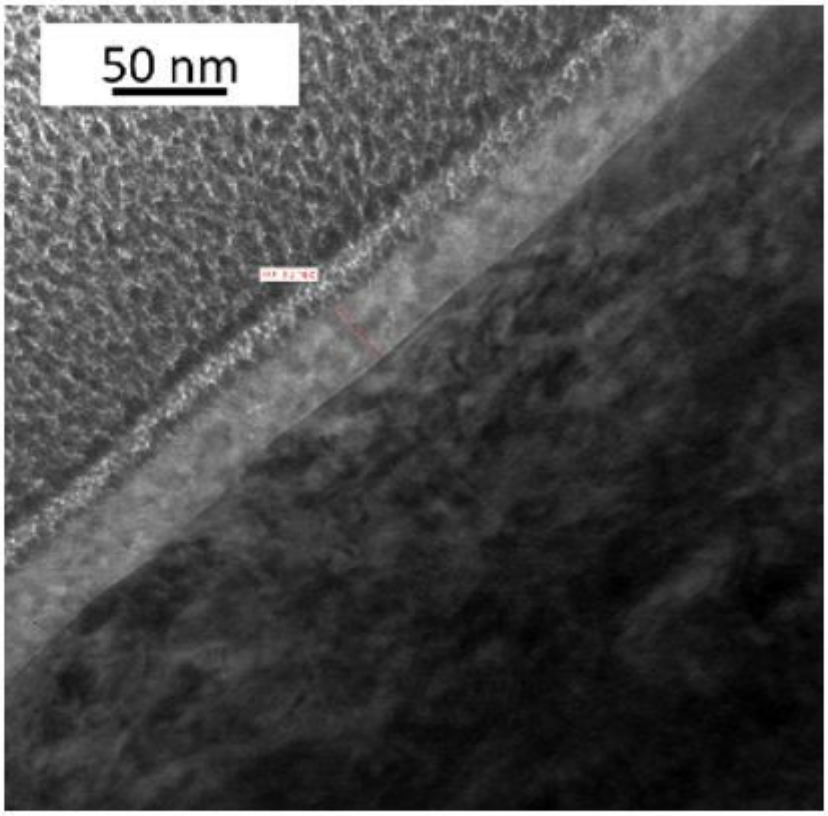

Figure 10

Cross sectional TEM micrograph illustrating an intact portion of the roller surface lubricated with PAO4+1% ZrO2 at 30% SRR after 119h of testing (Experiment 2). The ZrO2 tribofilm is covering the steel surface. No visible damage of the near subsurface (300 nm) is observed.

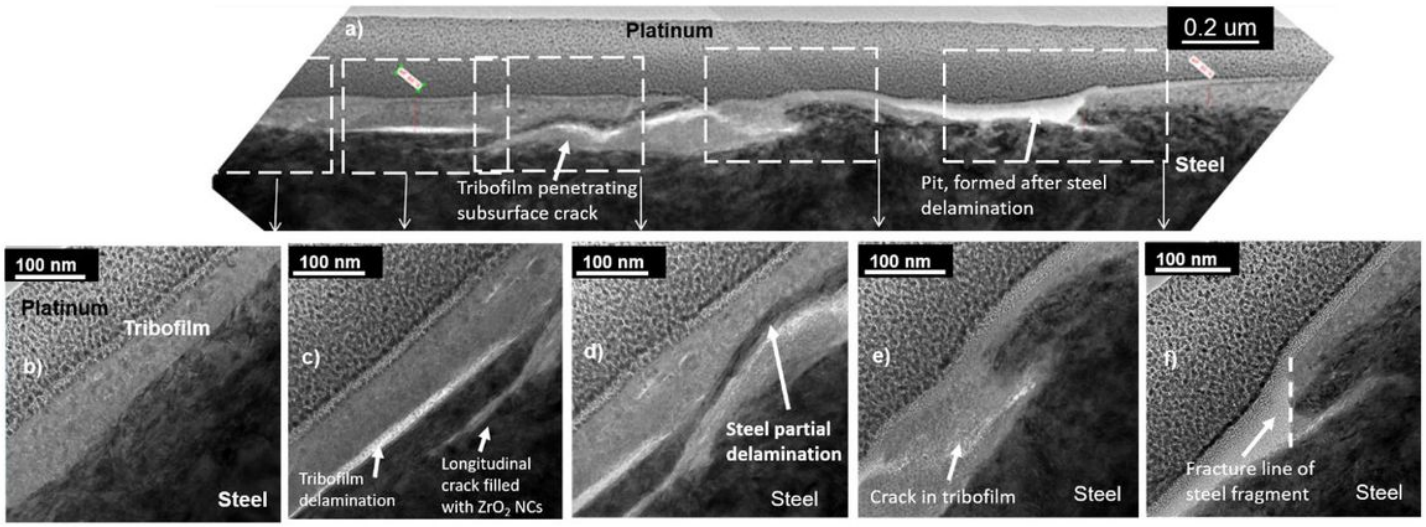

Figure 11

Cross sectional TEM micrographs from a roller tested at 30% SRR during 119h using PAO4+1% ZrO2 lubricant (Experiment 2). (a) Overview of a part of the TEM lamella showing alterations of the sub-surface of the roller. (b) Illustration of areas protected by ZrO2 tribofilm without any subsurface damages. (c) and (d) Delamination of a steel layer giving rise to a longitudinal crack. ZrO2 nanocrystals enter into the crack and stop its propagation. (e) shear-induced cracking of the tribofilm. (f) Lateral surface crack.

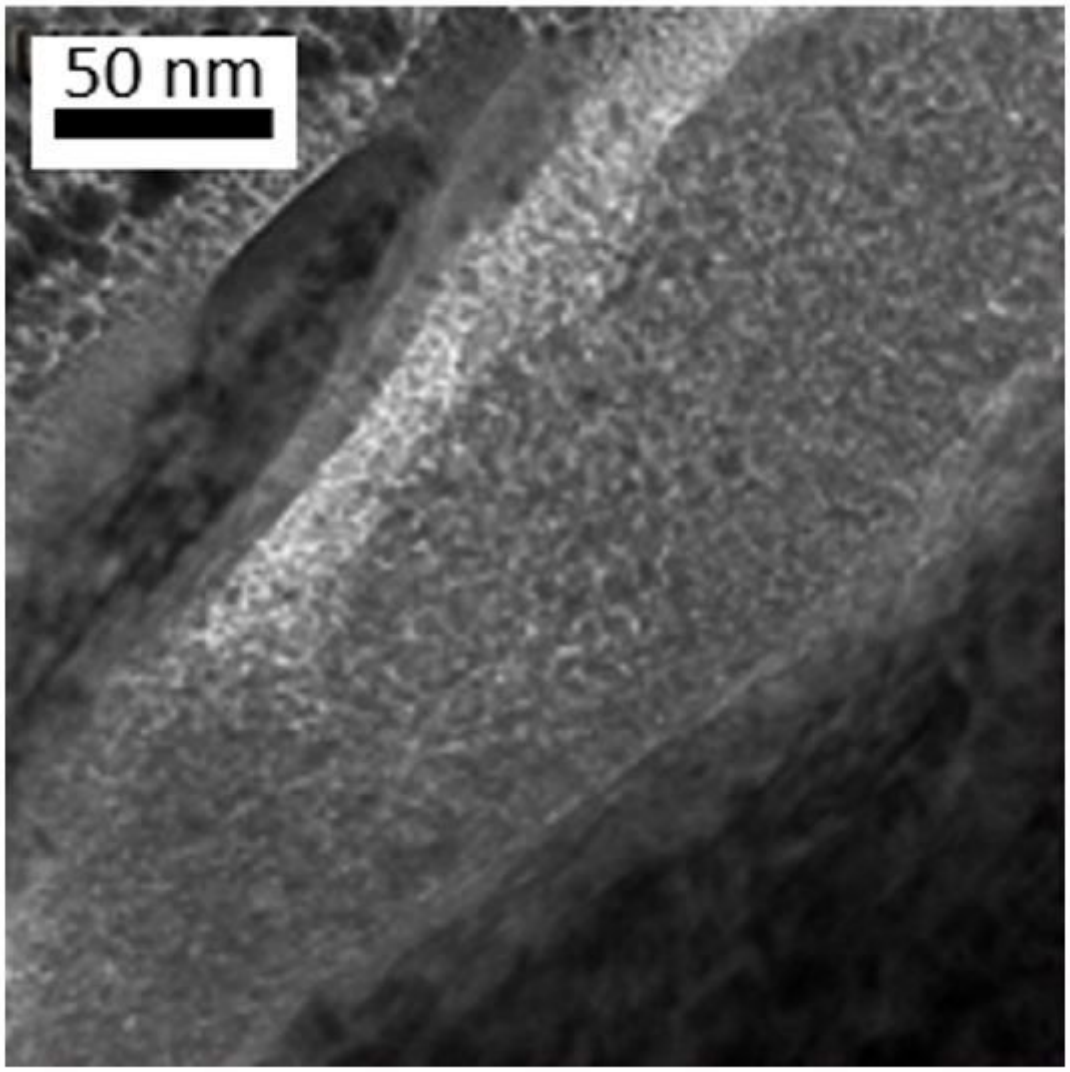

Figure 12

TEM micrograph illustrating the ability of 5 nm ZrO2 NCs to penetrate well inside the cracks. From Experiment 2.

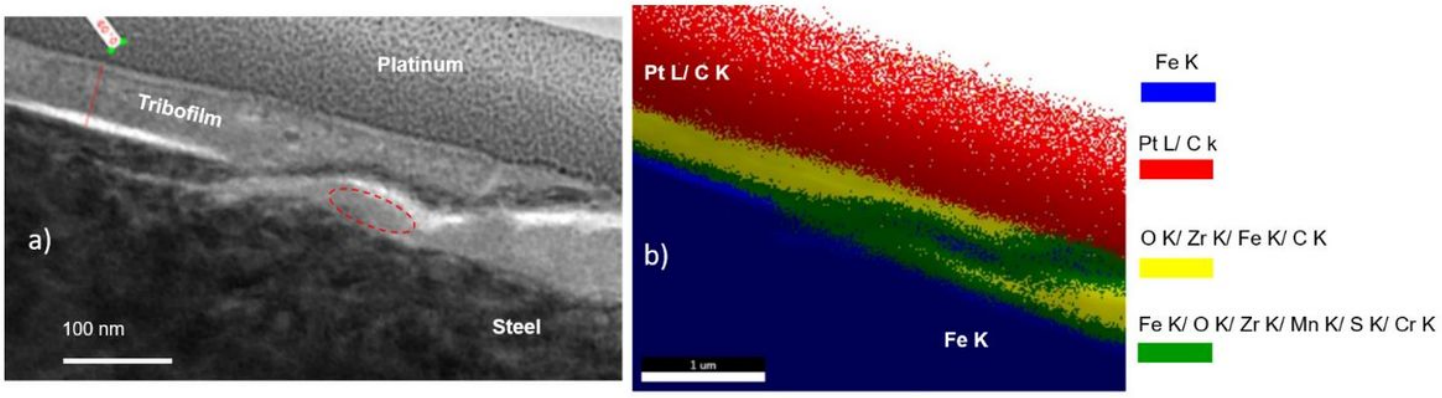

Figure 13

Cross sectional TEM micrograph from a roller tested at SRR 30% after 119h (Experiment 2) and its corresponding pixel reconstruction of a chemical mapping. (b) The pixel reconstruction is showing 4 phases: in red (the protective platinum coating), in yellow (the ZrO2 tribofilm), in blue (the steel substrate) and in green (phase around the crack rich in manganese, sulfur and chromium). The dashed oval in a) indicates the possible location of a MnS inclusion.

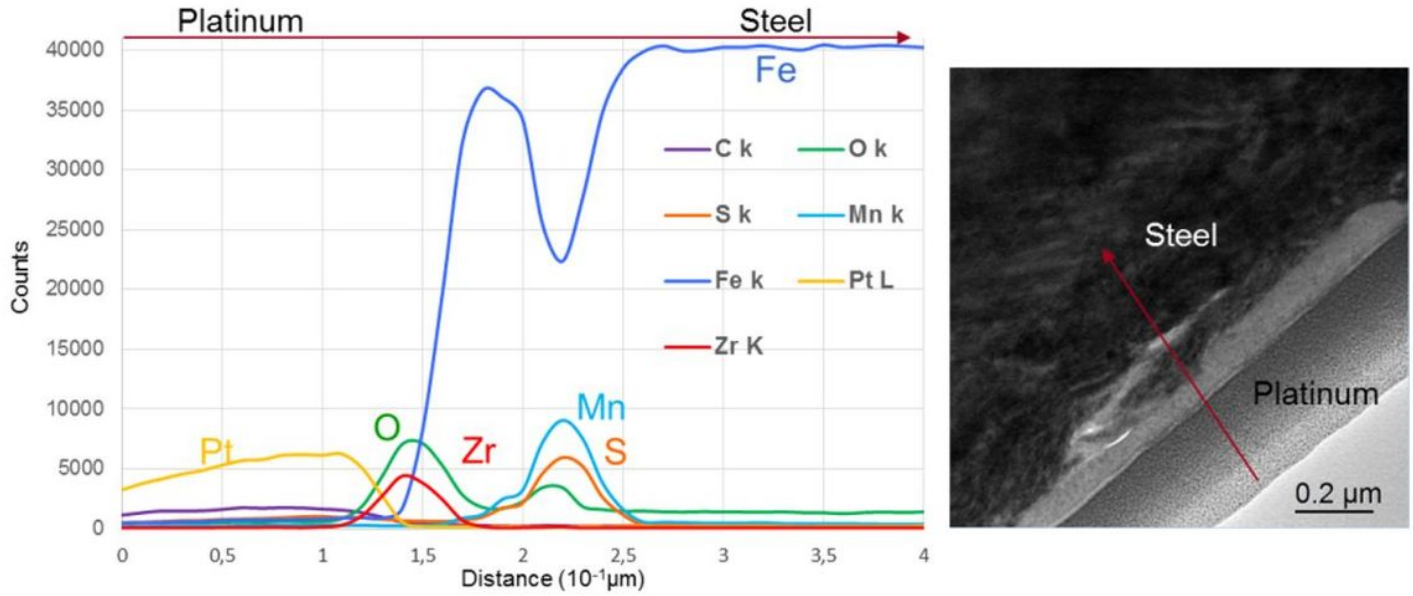

Figure 14

EDS depth profile across the subsurface crack observed in (b) showing a pic of Mn and S in the bright area inside the crack. The red arrow indicates the scan line of the profile. From Experiment 2.

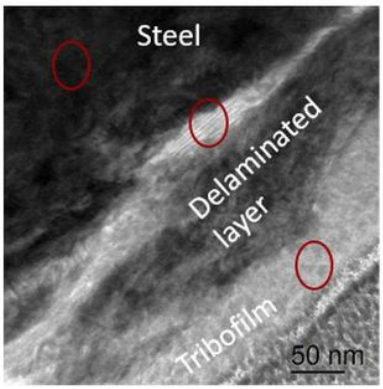

At%	O k	Zr K	C K	Mn K	S K	Cr K	Fe K
Inside cracks	20	1.2	3.8	9.4	6.3	1.2	58
Steel	0.8	--	2.5	0.7	0	1.7	97.3
Tribofilm	55	31	7	0	0.5	0.5	6

Figure 15

Atomic quantification of the composition of the inside crack areas in comparison with the composition of the steel substrate and ZrO2 tribofilm. From Experiment 2.

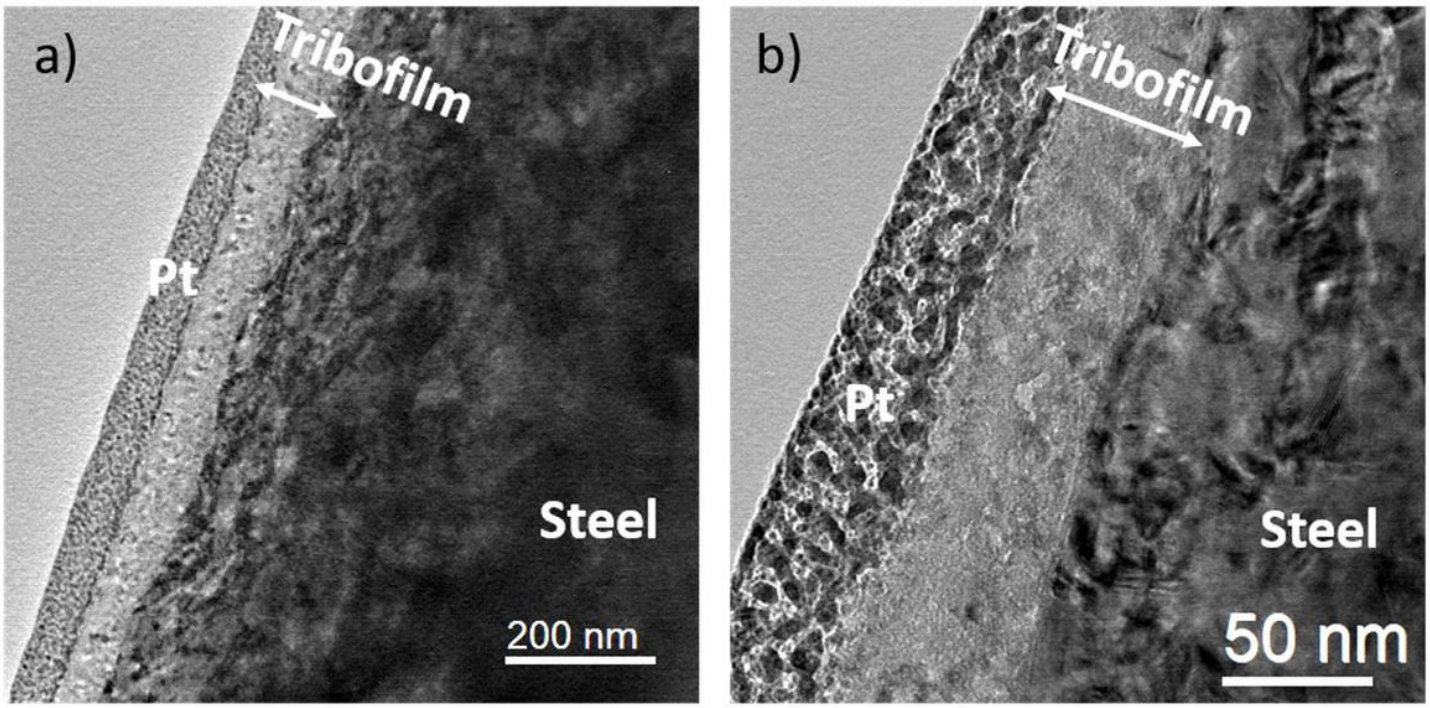

Figure 16

Cross sectional TEM micrographs from a roller tested at 0% SRR for a duration of 24h From Experiment 4. The zirconia tribofilm of a thickness of 70 nm ensures the roller surface integrity: absence of any damages or subsurface cracks. Note that the interface of steel is not as sharp as the ones tested at SRR 30%.

Supplementary Files

This is a list of supplementary files associated with this preprint. Click to download.

- EthicalStatement.pdf